EX/P6-30

High harmonic fast wave heating and beam driven ion cyclotron emission behavior in the LHD

H. Kasahara 1), K. Saito 1), T. Seki 1), R. Kumazawa 1), S. Kubo 1), T. Shimozuma 1), H. Igami 1), Y. Yoshimura 1), H. Takahashi 1), T. Mutoh 1), T. Oosako 2), Y. Takase 2), M. Ichimura 3), M. Osakabe 1), S. Ohdachi 1), M. Nishiura 1), K. Ida 1), T. Tokuzawa 1), I. Yamada 1), K. Narihara 1), S. Morita 1), H. Yamada 1), A. Komori 1), S. Sudo 1), O. Motojima 1) and the LHD experimental group1)

1) National Institute for Fusion Science, Toki 509-5292, Japan
2) University of Tokyo, Kashiwa, 277-8561, Japan
3) University of Tsukuba, Tsukuba 305-8571, Japan
e-mail contact of main author:kasahara.hiroshi@LHD.nifs.ac.jp

Abstract. Central electron heating with 40 % of heating efficiency is achieved by the use of high harmonic fast wave (HHFW) in the large helical device (LHD), and a substantial electron heating is observed in the central region of the plasma due to the synergy effect of ECH and HHFW. On the other hand, in high ion temperature aimed discharge ion cyclotron emissions (ICEs) are clearly detected using ion cyclotron heating antennas as a magnetic fluctuations, and the damped mechanism of ICEs is similar to that of HHFW. Observed magnetic fluctuations are rapidly increased after parallel NB is injected, and the excitation effect of ICEs seems to be different between fundamental and multi-harmonic ICEs in the direction of parallel NBI. When parallel NBI to counter direction is stopped, decay time of the fundamental ICE intensity is obviously longer than those of the higher harmonic ICE intensities.

1. Introduction

The Large Helical Device (LHD) has the largest helical superconducting coil all over the world [1], and stable plasma is produced without plasma current. A magnetic axis R_{ax} can be controlled while plasma shape kept constant, and plasma volume is approximately 30 m^3. In ordinary operation, the applied magnetic field B is less than 2.95 T at R_{ax} = 3.6 m (the device design value is 3 T), and ICRF (the range of frequency is from 25 to 100MHz.), ECRF (four frequencies, 77, 82.6, 84 and 168 GHz, are prepared.) and NBI (there are two kinds of beam sources (positive and negative ions) and injection directions (parallel and perpendicular to magnetic filed).) are equipped for auxiliary heating sources. In the LHD ion temperature at plasma center reaches over 5 keV [2], and central electron density (~ 4.6 x 10^{20} m^{-3}) over Greenwald limit is achieved [3]. To realize helical reactor like FFHR [4], an achievement of these parameters is necessary at the same time, and an establishment of central plasma heating method in high density and high temperature plasmas is key issue.

High harmonic fast wave heating (HHFW) has been considered to be one of the useful approaches to heat electrons at plasma center in the high density and high beta plasmas. In high beta plasmas like spherical tokamaks [5], effective electron heating is demonstrated in NSTX [6], and electron temperature reaches 3.9 keV from below 1 keV with 2.5 MW of HHFW power and with high single-pass damping. Main bulk electron heating mechanism of HHFW is electron landau damping (ELD) and transit time magnetic pumping (TTMP). Strong heating region is not related to cyclotron resonances because higher harmonic ion cyclotron damping is negligible [7], and HHFW is damped at ζ_e (phase velocity/electron thermal velocity) of 1. Electron heating experiments using HHFW are challenged in the LHD, and clear electron heating is observed with a few % of electron beta [8].

On the other hand, when perpendicular neutral beam is injected, ion cyclotron emissions (ICEs) [9] are clearly detected in the LHD [10]. ICE is fast wave with the multi-harmonic ion cyclotron frequencies, and damping mechanism of ICEs is similar to that of HHFW.

According to theoretical prediction of excitation mechanism of ICEs [11], excitations of ICEs are strongly related to be non-relaxed distribution functions, when the distribution function is increased with respect to the perpendicular velocity at plasma edge. Experimental results in tokamaks [12-14] are consistent with that theoretical prediction. In the LHD, magnetic field dependence of ICE frequencies and the excitation relationship between ICEs and perpendicular NBI are clearly observed, and they are similar to tokamak experimental results. In high ion temperature aimed operations, ICE intensities are rapidly increased after parallel NB is injected, and this behavior is very interesting because the power of direct perpendicular heating source is not changed.

In section 2, experimental setup of ICRF antennas for high harmonic fast wave heating and ion cyclotron emission detection is described. In section 3, focusing on the wave damping of high harmonic fast wave, the electron heating profile and the heating efficiency is discussed. In section 4, spectrum content of magnetic fluctuations is shown in high ion temperature aimed discharge, and the ICE intensities and the birth and decay time are discussed when parallel NB is injected. Finally, these conclusions and discussions are summarized in section 5.

2. Experimental setup - Fast wave excitation and detection using high power ion cyclotron heating antennas

In the LHD six antennas for high power ICRF heating are installed at different toroidal port (3.5U&L port, 4.5U&L port and 7.5U&L port), and four antennas (at 3.5 U&L port and 7.5 U&L port) are connected to high power ICRF amplifier through an impedance matching circuit [15]. In these antennas two pairs of ICRF antennas at 4.5 U&L port are used for excited wave detection because the high power transmission line is not constructed. The structure of six antennas is roughly same except minor changes, and the characteristic of wave excitation and detection is similar.

The ICRF antenna consists of single strap with faraday shield and carbon protectors, and the detail size as follows: strap width of 30 cm, strap height of 70 cm and loop length between back-plate and strap is approximately 10 cm. Fast wave is excited by single-loop-strap, and the excitation wave with small wavenumber $k_{\parallel}$ to magnetic field is bigger than that with large $k_{\parallel}$. These antennas are designed for effective minority heating [16], and high antenna loading is expected in small $k_{\parallel}$ excitation. Though these antennas are not optimized for HHFW heating, large $k_{\parallel}$ wave excitation is expectable since these antennas have wide strap and large loop region (~

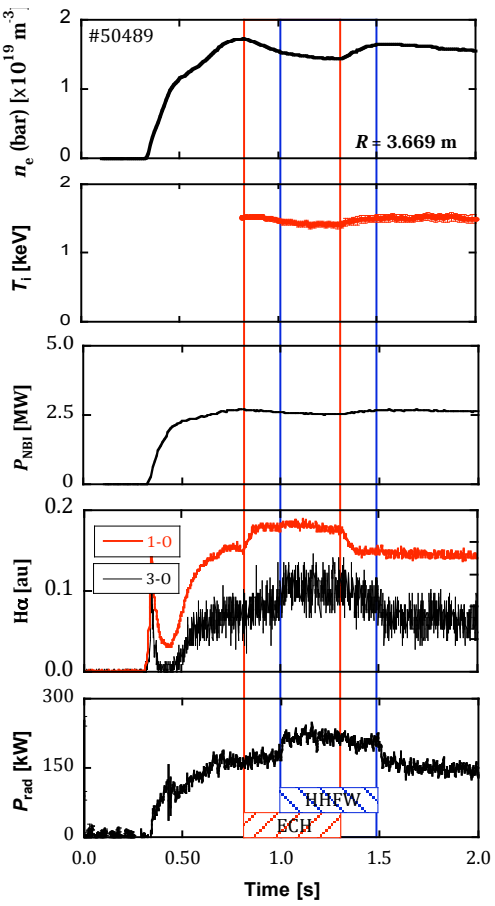

FIG. 1. These time evolutions of various plasma parameters during 2nd electron cyclotron wave heating (ECH) and high harmonic fast wave (HHFW) heating. A line integrated electron density (at R = 3.669 m), an ion temperature using Doppler broadening of Ar XVII, a deposition power of parallel NBI, Hα intensities at different toroidal positions (at 1-O port and 3-O port (near antennas)), a radiation power of soft x-ray with ECH and HHFW injection timings.

600 cm^2). A sensitivity as a magnetic fluctuation detector using single-loop-coil is proportion to the loop area, and ICRF antennas are good sensitivity probe [17]. In this experiment magnetic fluctuations are measured using ICRF antennas at 4.5 U&L ports, and the signal of magnetic fluctuations is recorded by an oscilloscope with a maximum sampling rate of 500 MHz. Typically, signals are sampled for 100 μs in every 15 ms such a discrete sampling method.

3. Fast wave damping for electron heating

3.1. High harmonic fast wave heating in the helical plasma

In the LHD a synergy effect of ECH and HHFW is observed with weak single-pass damping of HHFW, and a direct electron heating is observed using HHFW. This target plasma (50488, 50489) is produced by NBI (from t = 0.3 s to t = 2.3 s) and ECH (from t = 0.8 s to t = 1.3 s), with parameters as follows: a magnetic field B of 1.5 T, a magnetic axis R_{ax} of 3.6 m, a line integrated electron density n_e of 1.7 x 10^{19} m^{-3} at R = 3.67 m and a central electron temperature T_e of 2.5 keV. HHFW is injected with a RF power of P_{HHFW} = 1.6 MW from t = 1.0 s to t = 1.5 s (50489).

Figure 1, 2 and 3 show the time evolution of various plasma parameters during HHFW heating. When ECH is injected at t = 0.8 s, a line integrated electron density, a deposition power of parallel NBI and a stored energy using diamagnetic coil are gradually decreased. An intensity of good sensitive Hα signal at 1-O port is simultaneously increased during ECH, and an intensity of Hα signal at 3-O port, which is near ICRF antennas at 3.5 ports, is increased during HHFW. A radiation power of soft x-ray and the Hα intensity at 3-O port is increased at the timing of ECH and HHFW injection, and plasma heating is carried out without bad impurity increment. Figure 2 shows an averaged electron temperature T_e from major radius R = 3.4 m to R = 3.6 m using Thomson scattering diagnostic. Comparing reference plasma (50488) with HHFW heated plasma (50489), clear central electron heating is observed during electron cyclotron heating (ECH) and high HHFW heating (see Fig. 2). When ECH is stopped at t = 1.3 s, central electron temperature is decreased though HHFW has been injected. The trend of electron temperature is similar to that of Hα at 3-O port, and it suggests that effective heating in front of antenna is achieved during ECH heating. This result supports the synergy effect of ECH and HHFW heating. Considering no clear electron heating evidence around t = 1.5 s (50489), collaboration

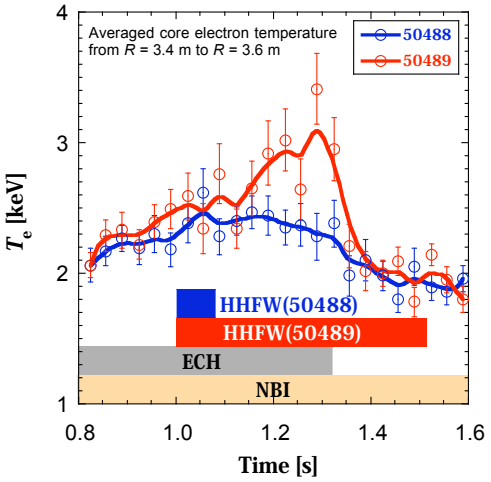

FIG. 2. The time evolution of an averaged central electron temperature T_e from R = 3.4 m to R = 3.6 m using Thomson scattering diagnostic. Clear electron heating is achieved when both of ECH and HHFW is injected.

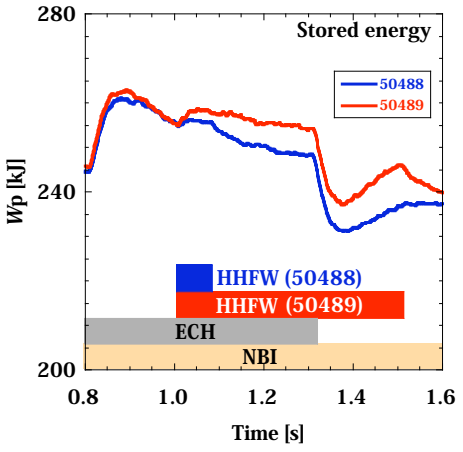

FIG. 3. The time evolution of a plasma stored energy W_p using diamagnetic coil. When auxiliary heating power is injected or stopped, clearly discontinuity points of W_p appear at t = 1.0 s, 1.3 s and 1.5 s.

with ECH and HHFW heating is important. Heating efficiency of HHFW is estimated at HHFW injection timing using break-in-slope method in Fig. 3, and that calculated efficiency is approximately 50 %.

3.2. Electron heating region using electron cyclotron emission diagnostics

Figure 4 shows the time evolution of electron temperatures using electron cyclotron emissions from near plasma center to plasma edge. There are two HHFW injection pulses, first pulse is from t = 0.8 s to t = 1.0 s without ECH assist, and second pulse is from t = 1.2 s to t = 1.4 s with ECH assist. A line integrated electron densities on each HHFW injection timing are approximately same, 0.5 x 10^{19} m^{-3}, and in first HHFW injection an increase of electron temperature at ρ = 0.14 is not clear. Second hydrogen cyclotron resonance exists near $\rho \sim 0.5$ in B = -1.5 T at R_{ax} = 3.6 m, and it is possible to heat electron by second ion harmonic heating in ion-electron relaxation time [18]. Second harmonic fast wave heating is strongly damped to electron [19, 20], and the heating position is close to ion cyclotron resonances (off-axis). On the second HHFW pulse, electron temperature at ρ = 0.14 (near center) is simultaneity increased. HHFW heating efficiency to electrons is strongly related to an electron beta, and directly central electron heating is expectable. These results seem to be off-axis electron heating in that first pulse (without ECH assist) and central electron heating in the second pulse (with ECH assist). The collaboration between ECH and HHFW is important for effective central heating in the LHD.

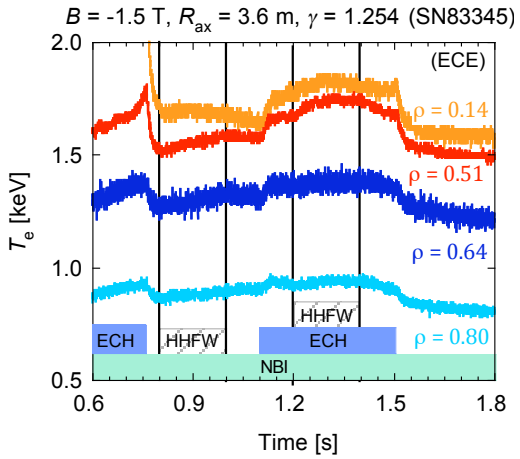

FIG. 4. The time evolution of electron temperatures using electron cyclotron emissions at ρ = 0.14, 0.51, 0.64 and 0.80. Two pulses of HHFW are injected at t = 0.8 s and t = 1.2 s, and HHFW power is approximately 1 MW. Line integrated electron densities near plasma center at each HHFW pulse injections is approximately 0.5x10^{19} m^{-3}, and a parallel NBI power is less than 3MW.

3.3. Electron heating estimation

HHFW heating efficiency was investigated to study the lower density dependence for weak single-pass damping with central temperature around T_e = 1.7 keV to T_e = 2.3 keV. Figure 5 shows HHFW heating efficiency estimated by a break-in-slope method using diamagnetic coil. In these discharges, the heating efficiency of HHFW increases up to 0.6 as the electron density increases, and it seems that heating loss for multi-pass damping is small since calculated single-pass damping is less than a few %.

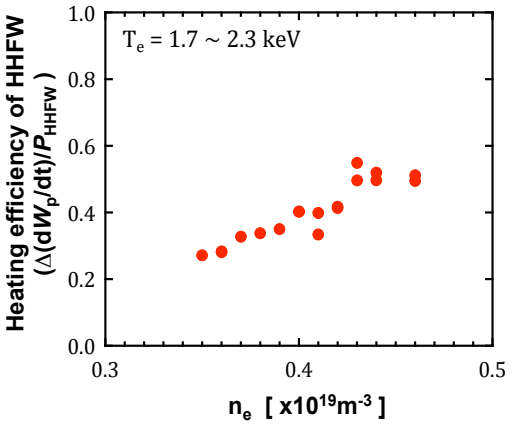

FIG.5. The HHFW heating efficiency for various central low line integrated electron densities with ECH assist, and preferable heating efficiency (~ 60 %) was achieved though a single-pass damping of HHFW is less than a few %.

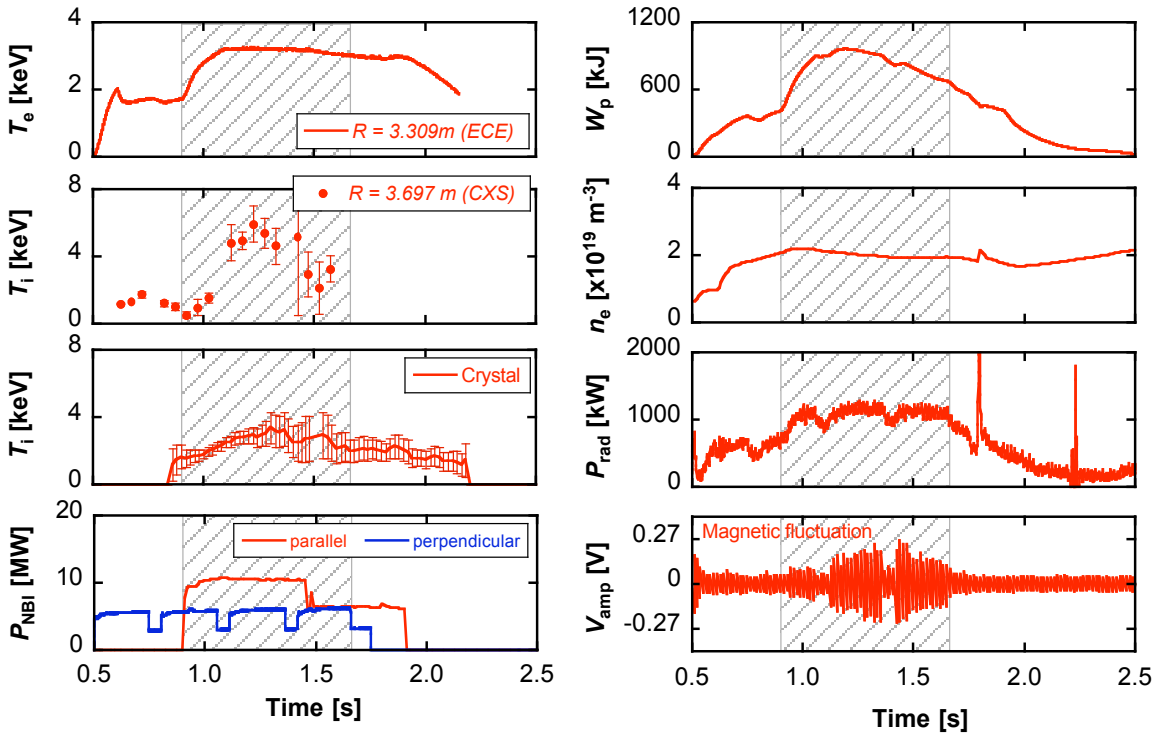

FIG. 6. Typical plasma parameters in high ion temperature aimed discharge. An electron temperature T_e near plasma center using ECE diagnostic, ion temperatures using CXS and crystal spectrometer, neutral beam injection powers to parallel and perpendicular direction, a stored energy using diamagnetic coil, a line integrated electron density using FIR diagnostic, a radiation for soft x-ray and magnetic fluctuations using ICRF antenna.

4. Fast wave excitation driven by high-energy particles

4.1. High frequency wave observation using ion cyclotron frequency antenna

Figure 6 shows typical plasma parameters in high ion temperature aimed discharge (80268) in B = -2.77 T at R_{ax} = 3.575 m, and ion temperatures T_i is measured by charge exchange recombination spectroscopy diagnostic (CXS) [21] near plasma center (at R = 3.697 m) and crystal spectrometer diagnostic (Crystal) using Doppler broadening of Ar_{XVII} line intensity. ECH is used for initial plasma production from t = 0.3 s to t = 0.7 s, and perpendicular NB is injected for plasma sustainment. Ion and electron temperatures near plasma center is roughly same before parallel NB is injected, and a line integrated electron density is kept constant from t = 0.9 s to t = 1.7 s. Compared electron and ion temperature with stored energy, stored energy is strongly related to be ion temperature using CXS because electron temperature is kept constant after t = 1.5 s. When ion temperature at plasma center goes over approximately 4 keV, ion temperature measured by Crystal is underestimated since line emission of Ar at plasma center is much weaker than that at $\rho > 0.5$.

Magnetic fluctuations using ICRF antenna are increased from t = 0.5 s to t = 1.75 s, and the region from t = 0.9 s (the start timing of parallel NBI) to t = 1.7 s (the power decreased timing of perpendicular NBI) is hatched in Fig. 6. In the hatched region, magnetic fluctuations are increased as stored energy and plasma temperature near center are increased, and observed magnetic fluctuations seem to be strong relation to the timing of parallel NB is injected.

4.2. Detected magnetic fluctuation spectrums in high ion temperature aimed operation

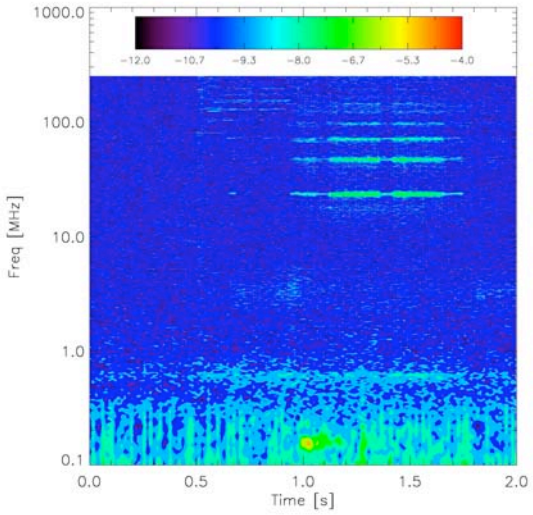

FIG. 7. The detected magnetic fluctuation spectrum. The vertical axis is frequency from 100 kHz to 200 MHz, and the horizontal axis is time from t = 0 s to t = 2 s. Colours are related to spectrum powers, and the values on colour chart-bar mean the exponential part of spectrum power. For example, Red is 10^{-4} [au], and black is 10^{-12} [au].

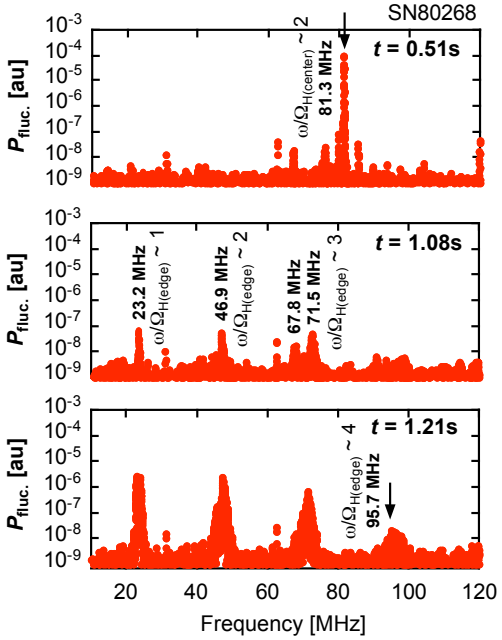

FIG. 8. ICE spectrums in three auxiliary heating timings. ECH: t = 0.51 s, parallel NBI: t = 1.08 s and achieved high ion temperature timing: t = 1.21 s.

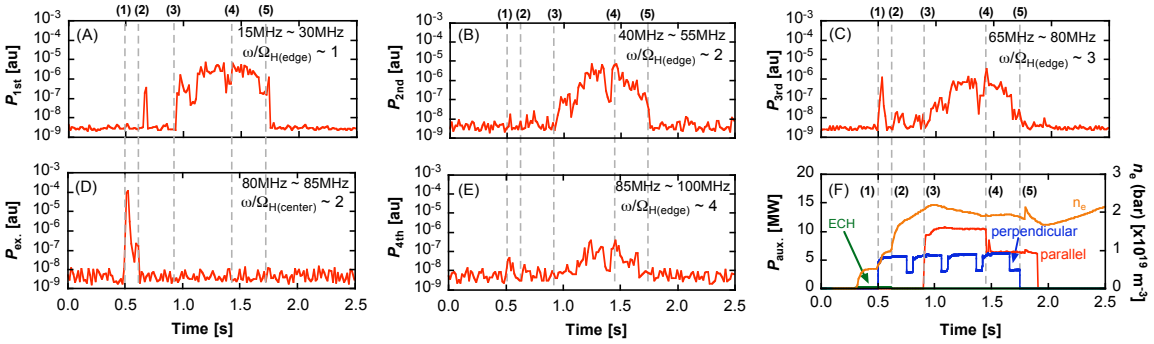

FIG. 9. The time evolution of spectrum peaked intensities in various ICE frequencies (15 ~ 30 MHz, 40 ~ 55 MHz, 65 ~ 80 MHz, 80 ~ 85 MHz, 85 ~ 100 MHz). In these frequencies region, main peaked frequency is as follows: 23 MHz ($\omega/\Omega_{H(edge)}^{1st}$), 47 MHz ($\omega/\Omega_{H(edge)}^{2nd}$), 72 MHz ($\omega/\Omega_{H(edge)}^{3rd}$), 81 MHz ($\omega/\Omega_{H(center)}^{2nd}$) and 96 MHz ($\omega/\Omega_{H(edge)}^{4th}$). Five typical auxiliary heating timings (dashed-lines) are shown, and perpendicular NB with 4 MW is injected from t = 0.5 s to 1.75 s. The other auxiliary heating timing is as follows: (1): perpendicular NBI is started, (2): ECH is stopped, (3): parallel NBI is started, (4): parallel NBI power is decreased and (5): perpendicular NB injection is stopped.

Figure 7 and 8 show power spectrum of high frequency magnetic fluctuation using 4th Blackman-Harris filter, and many characteristic spectrum peaks are detected at three timings as follows: plasma production timing with poor electron density (t = 0.51 s), just after parallel NBI (t = 1.08 s) and achieved high ion temperature (t = 1.21 s). These clear main spectrum peaks in Fig. 8 are ICEs, and those excited waves seem to come from near magnetic axis and plasma edge in plasma production timing. Except the strong fluctuation (160 kHz) around t = 1.0 s, intensities of observed magnetic fluctuation under frequencies of 1 MHz aren't changed in Fig. 7, and the intensity with 160 kHz of frequency around t = 1.0 s in Fig. 6 is smaller than

the other intensities of ICE at around t = 1. 5 s. The wave content of direct observed magnetic fluctuation in Fig. 6 seems to be ICEs in the hatched region.

In very low electron density plasma such as a calibration discharge of perpendicular NBI power deposition, a frequency peak of 40 MHz is detected, and the excitation region seems to be plasma center on the magnetic axis. The detected wave having frequency of 81 MHz seems to be a second harmonic ICE, and the excited region is near magnetic axis. On the other hand, the others (frequencies of 23, 47, 72, 96 MHz) are ICEs, which are excited around midplane edge and they are consistent with previously observed ICE [10]. Compared these spectrum peaks at t = 1.08 s with those at t = 1.21 s, frequencies of main spectrum peaks are not changed, though a wave with 67.8 MHz of frequency is vanished at t = 1.21 s. Since main observed frequencies are not changed after t = 1 s, these main excitation regions are plasma edge and they are not changed.

4.3. Relationship between ICE intensities and auxiliary heating

Figure 9 shows the time evolution of various peaked ICE intensities in five frequencies region ((A): 15 ~ 30 MHz, (B): 40 ~ 55 MHz, (C): 65 ~ 80 MHz, (D): 80 ~ 85 MHz and (E): 85 ~ 100 MHz) at different heating timing ((1): ECH, (2): perpendicular NBI only, (3): parallel NBI + perpendicular NBI, (4): parallel NBI power is decreased and (5): perpendicular NBI is stopped). Strong relationship between peaked ICE intensities and auxiliary heating timing is observed in Fig. 9. In plasma production phase (1), the excitation of a fundamental ICE (23 MHz, $\omega/\Omega_{H(edge)}^{1st}$) is unclear, and second harmonic ICE (81 MHz, $\omega/\Omega_{H(center)}^{2nd}$) near plasma center and third harmonic ICE (72 MHz, $\omega/\Omega_{H(edge)}^{3rd}$) at plasma edge are instantaneously excited. The birth times of ICEs are much shorter than particle slowing down time. These intensities of second and third harmonic ICEs are rapidly decreased after these ICEs are just excited, and the third harmonic ICE intensity is disappeared before ECH is stopped. Just after ECH is stopped (2), the second harmonic ICE intensity is simultaneously disappeared, and the production of second harmonic ICE seems to be strongly related to be ECH at plasma center.

When parallel NB is additionally injected from t = 0.9 s on perpendicular NBI (3), the intensity of $\omega/\Omega_{H(edge)}^{1st}$ is instantaneously increased. The birth time of $\omega/\Omega_{H(edge)}^{1st}$ is much smaller than the other birth times of multi-harmonic ICEs (2nd, 3rd and 4th) at plasma edge, and the time is short such as a particle lost time [10]. For theoretical prediction, the excitation mechanism of ICEs is strongly related to narrow ion distribution of parallel velocity to the magnetic field, and such a distribution is likely to occur around midplane edge of the plasma close to the point of perpendicular NBI [22]. They are consist with observed time and point of $\omega/\Omega_{H(edge)}^{1st}$.

Considering the time evolution for intensities from 1st to 4th ICEs, the suppressed intensity times for ICEs are roughly same, though these growth rates are different in ICE harmonics. These suppression times of ICE intensities are obviously longer than the energy confinement time and particle lost time, and narrow ion distribution with large perpendicular velocity at plasma edge seems to be increased when parallel NB is injected.

When parallel NBI power to counter direction is stopped at t = 1.45 s (4), all ICE intensities (from 1st to 4th harmonics) are gradually decreased. Decay times of ICE intensities from 2nd to 4th harmonics are similar to those suppression times, and there are clearly different between decay time and suppression time of fundamental ICE. The direction of parallel NBI plays a key role in the decay time of ICEs from 2nd to 4th, and in fundamental ICE the effects are not strong since the decay time is much longer than the other decay times of ICEs (from 2nd to 4th).

5. Summary

In the LHD clear electron heating is achieved using HHFW, and electron temperature near plasma center is increased with ECH assist. Single-pass damping is a few %, which is much smaller than that of tokamak experiments [6, 23, 24], and the optimization of direct bulk electron heating is needed without ECH assist in the LHD. ECH assists the achievement of effective HHFW heating, and ECH heated electrons at plasma center seem to be strongly related to HHFW heating.

Perpendicular NBI driven ICEs are clearly observed in the LHD, ICEs intensities are gradually increased when parallel NB is injected. Excited positions of ICEs are around midplane edge of the plasma close to the point of perpendicular NBI, and the excited point of experimental result is consistent with theoretical prediction. When parallel NBI to counter direction is stopped, multi-harmonic ICE intensities are decreased. Multi-harmonic ICE excitations seem to be related the orbits driven by parallel NBI to counter direction. The effect is weak in fundamental ICE excitation, and the decay time of fundamental ICE is obviously longer than those decay times of multi-harmonic ICEs.

Acknowledgment

The authors would like to thank the scientists, the engineering and the technical stall at the National Institute for Fusion Science, who made these experiments possible. This work is supported by the NIFS budget NIFS06ULRR504, NIFS07ULRR504, NIFS07ULRR06 and NIFS07ULRR08.

Reference

[1] Iiyoshi A. et al., *Nucl. Fusion* **39** (1999) 1245.
[2] Yokoyama M. et al., *Phys. Plasmas* **15** (2008) 056111
[3] Motojima O. et al., *Nucl. Fusion* **47** (2007) S668.
[4] Sagara A. et al., *Fusion Eng. Des.* **81** (2006) 2703.
[5] Peng Y-K.M. and Strickler D. J., *Nucl. Fusion* **26** (1986) 769.
[6] LeBlanc B.P. et al., *Nucl. Fusion* **44** (2004) 513.
[7] Ono M. et al., *Phys. Plasmas* **2** (1995) 4075.
[8] Kasahara H. et al., *Journal of the Korean Physics Society* **49** (2006) S192.
[9] Dendy R.O. et al., *Nucl. Fusion* **35** (1995) 1733.
[10] Saito K. et al., *submitted to Fusion Eng. Des.*
[11] Dendy R.O. et al., *Nucl. Fusion* **1** (1994) 3407.
[12] Cauffman S. and Majeski R., *Nucl. Fusion* **35** (1995) 1597.
[13] McClements K.G. et al., *Phys. Rev. Lett.* **82** (1999) 2099.
[14] Seki M. et al., *Phys. Rev. Lett.* **62** (1989) 1989.
[15] Kumazawa R. et al., *Rev. Sci. Ins.* **70** (1999) 2665.
[16] Mutoh T. et al., *Nucl. Fusion* **43** (2003) 738.
[17] Kasahara H. et al., *submitted to Rev. Sci. Ins.*
[18] Saito K. et al., *Plasma Phys. Control. Fusion* **44** (2002) 103.
[19] Kimura H. et al., *Plasma Phys. Control. Fusion* **35** (1993) 845.
[20] Rogers J. H. et al., *Fusion Energy 1996* **4** (1997) 317.
[21] Ida K. et al., *Rev. Sci. Ins.* **79** (2008) 053506.
[22] Dendy R.O. et al., *Nucl. Fusion* **1** (1994) 1918.
[23] Heidbrink W.W. et al., *Nucl. Fusion* **39** (1999) 1369.
[24] Pinsker R.I. et al., *Nucl. Fusion* **46** (2006) S416.